Multi-GPU based 3D numerical modeling of fluid migration and clay dehydration influence on Lusi hydrothermal activity (Java, Indonesia)

Reza Sohrabi, Benjamin Malvoisin, Adriano Mazzini, Stephen Miller

To cite this version:

Reza Sohrabi, Benjamin Malvoisin, Adriano Mazzini, Stephen Miller. Multi-GPU based 3D numerical modeling of fluid migration and clay dehydration influence on Lusi hydrothermal activity (Java, Indonesia). Journal of Volcanology and Geothermal Research, 2021, 419, pp.107377. 10.1016/j.jvolgeores.2021.107377 . hal-03330652

1   **Multi-GPU based 3D numerical modeling of fluid migration and clay dehydration influence**

2   **on Lusi hydrothermal activity (Java, Indonesia)**

3   Reza Sohrabi [a,*], Benjamin Malvoisin [b], Adriano Mazzini [c], Stephen A. Miller [a]

4   [a] Centre for Hydrogeology and Geothermics (CHYN), University of Neuchâtel, Neuchâtel, Switzerland

5   [b] Institut des Sciences de la Terre (ISTerre), Université Grenoble Alpes, CNRS, Grenoble, France

6   [c] Centre for Earth Evolution and Dynamics (CEED), University of Oslo, Oslo, Norway

7   [*] Corresponding author. E-mail address: reza.sohrabi@unine.ch (R. Sohrabi)

8

11

12   Highlights:

13   ➢ Couplings between fluid flow, heat transport and reactions in the Lusi system solved with multi-GPU technology

14   ➢ High-Performance Computing with 3D numerical models using multi-GPU processing

15   ➢ Fluid pressure build-up due to clay dehydration controls hydrothermal system fluid outflow

16

17   **Abstract**

18   The Lusi mud eruption in East Java has been active since May 2006. Magma emplacement at depth,

19   clay dehydration, and mud liquefaction during seismic wave propagation have been invoked as

20   mechanisms fueling this eruption. However, the respective roles of these processes are still poorly

21   constrained. In this focused study, we numerically investigate the influence of clay dehydration,

22   mass and heat transport on fluid outflow at the Lusi site using a fully coupled 3D model for this

23   active system. Using a multi-GPU parallel processing algorithm, we propose an estimate of the 3D

24   time evolution of pressure, temperature, porosity, permeability and water liberation in a large-scale

25   (9 km - 14 km - 5.5 km) deep hydrothermal system at high-resolution. Simulations indicate that

26   high-pressure fluids generated by dehydration reactions are sufficient to induce hydro-fractures that

27   would significantly influence the porosity and permeability structures. Dehydration is an essential

28   component for understanding the Lusi system, because the fluids generated contribute to the

29   outflow and may have a considerable impact for the maintenance of the infrastructure required to

30   keep the Lusi site safe. High-Performance Computing (HPC) offers high-resolution simulations for

31   studying time evolution of such natural systems, and potentially for geothermal resource

32   development for the surrounding population.

33

34

1 Introduction

3D numerical modeling is a powerful tool for investigating processes occurring in the Earth's interior such as hydrothermal circulation or geothermal exploitation. The dynamics of such complex systems involve coupled and nonlinear flow, heat transport and reaction. Quantitative analysis of these systems is challenging and relies on numerical solutions of coupled partial differential equations (PDEs). Considerable effort during the last decades focused on various algorithms for solving PDEs on multi-CPU platforms, but these algorithms have made limited use of evolving hardware changes such as GPU-computing. 3D numerical modeling of hydrothermal systems presents a major challenge due to the physical processes involved (Ingebristen et al., 2010; Jeanne et al., 2014) over both short and long-terms (White, 1957; Bowen, 1979; Ingebritsen & Sanford, 1999; Lowenstern & Hurwitz, 2008; Hurwitz & Manga, 2017). Scientific models have been developed for heat and mass transport through porous media with progressively more complex physics (White & Oostrom, 2003; Steefel et al., 2005; Bangerth et al., 2007; Zhang et al., 2008; Gaston et al., 2009; Flemisch et al., 2011; Kolditz et al., 2012; Hammond et al., 2014; Su et al., 2017). The need for predictive tools led to the development of reactive models considering reaction kinetics and reaction induced changes in porosity (Steefel et al., 2005; Lichtner & Carey, 2006; Lichtner & Kang, 2007; Xu et al., 2008). However, none of these have used multi-GPU technology.

The Lusi eruption (Java, Indonesia) provides an unprecedented opportunity to test large scale numerical modeling for a hydrothermal system at its infancy. This system, erupting since the 29th of May 2006 in East Java, elicited debate in science and politics (Van Noorden, 2006). During the early phases, a sequence of aligned clastic eruptions appeared through fractures that followed the same orientation as the Watukosek fault system, a NE-SW tectonic structure in NE Java (Figure 1). This structure can be observed from satellite images and exhibits fractures (including antithetic lineaments), in the field and on seismic data (Mazzini et al., 2009; Moscariello et al., 2018; Obermann et al., 2018; Sciarra et al., 2018; Mazzini et al., 2021). Fluids quickly flooded large parts of the Sidoarjo Regency urban area, permanently displacing 60,000 people (Richards, 2011). Fifteen years later, Lusi continues to erupt boiling mud breccia and displays perpetual geyser-like behavior (Karyono et al., 2017) with flow rates of ~ 80,000 m^3/day and, with significant earthquake-triggered increases, up to ~120,000 m^3/day (Miller and Mazzini, 2018; Mazzini et al., 2021). This system displays complex interactions between hydrothermal fluids and carbonate- and clay-rich formations in an active tectonic setting neighboring a volcanic complex.

Numerical modeling helps decipher the mechanisms involved in Lusi hydrothermal system formation and evolution. Mud flow is generally studied by considering a mud reservoir linked to the

surface by a mud filled conduit. Zoporowski and Miller (2009) reproduced the oscillatory behavior of the eruption with such a geometry. Rudolph et al. (2011) considered the effect of overpressure in the mud reservoir on flow through the conduit, and eruption longevity. Davies et al. (2011) also estimated the evolution of the eruption rate with time but with a probabilistic approach. Collignon et al. (2018) determined the influence of conduit radius and clast presence on flow velocity in the conduit. Numerical modeling was also used at Lusi to study other processes than mud flow. Istadi et al. (2009) studied the surface area affected by the eruption by combining topographic data with measured mud flow while considering processes such as faulting and subsidence. Svensen et al. (2018) used a one-dimensional thermal model to predict the influence of magma emplacement at depth on the emission of CO_2. Mazzini et al. (2009) studied the link between strike-slip faulting and fluidization with several rheological models. Tanikawa et al. (2010) modelled the generation of overpressure during diagenesis. All these models shed light on processes involved in the eruption. However, three-dimensional models were not developed, preventing the complex geological structure observed at Lusi (Mazzini et al., 2007) from being reproduced. Moreover, the contribution of heated fluids generated by magmatic intrusion emplacement and clay dehydration is still enigmatic.

This study investigates the evolution of the Lusi system by exploring hydrothermal fluid circulation and coupled hydro-thermo-mechanical interactions and its potential use for geothermal resources. We report on a series of numerical simulations using multi-GPU computing to model physical processes involved in this eruptive clastic system. We show that evolution of the Lusi hydrothermal eruption is likely connected to the generation of high fluid pressures by dehydration reactions as proposed by Mazzini et al. (2007, 2012, 2018) and petrographic data analyses (Malvoisin et al., 2018; Zaputlyaeva et al., 2020). These authors revealed that the clasts originating from the deepest sedimentary formation (i.e. Ngimbang Formation shale source rock) intersected by the Lusi conduit have been exposed to temperatures higher than 350°C. However, the Ngimbang Formation sediments have never been included in any numerical simulation representing the Lusi system. Our modeling shows that dehydration can generate a substantial overpressure and the fluids necessary to support eruption at Lusi. Our model represents the first attempt to model the couplings between reaction, deformation and fluid flow at high-resolution. Here we present a novel approach using models developed to simulate more than 7 billion numerical grid cells in a relatively short computational time (less than a week).

We explore this hypothesis with two different scenarios where in magmatic intrusion and related hydrothermal fluid migration at depth (500°C and 1,000°C beneath Lusi) induces dehydration within the sediment package and, ultimately, we quantify this contribution to the overall fluid

103　outflow. Finally, we investigate the influence of simple reactions and temperature changes on
104　porosity and fluid pressure to determine the evolution of fluid flow. The investigation of this
105　complex system requires the development of long-term computational multi-physics approaches at
106　high-resolution in three dimensions.

107

108　**2 Methodology and model set-up**

109　The local stratigraphy has been constrained from borehole data complemented by regional studies,
110　seismic data interpretations, and analysis of erupted clasts (Mazzini et al., 2007; Malvoisin et al.,
111　2018; Moscariello et al., 2018; Samankassou et al., 2018; Zaputlyaeva et al., 2020). The identified
112　units and formations have been used by Sohrabi et al. (2018) to propose the first 3D geological
113　model for the Lusi eruption: Altered sand, shale and clay from the Pucangan Formation (blue) in
114　Figure 2a, Bluish Grey clay from the Upper Kalibeng Formation (purple), volcanoclastics from the
115　Upper Kalibeng Formation (red), carbonates from the Kujung-(Prupuh)/Tuban Formations (orange),
116　and mudstones from the Ngimgbang Formation (yellow). The model also includes two major faults
117　or shear zones (red) crossing Lusi, the Watukosek strike slip system and the Siring antithetic faults
118　system (Figure 2a). This 3D heterogeneous geological numerical model is then implemented in a
119　newly developed numerical High-Performance Computing (HPC) tool for subsurface fluid
120　dynamics (Sohrabi et al., 2019). To our knowledge, there is no other numerical tool that can couple
121　physical processes such as clay dehydration, considering porosity and permeability evolution
122　through time, in three-dimensions at such high-resolution (more than 7 billion numerical cells).

123　Lusi is a sediment-hosted hydrothermal system connected at depth with a neighboring magmatic
124　complex located ~10 km to the SW (Miller and Mazzini, 2018). Geochemical studies show that
125　Lusi vents a mixture of gases that indicate formation temperatures of up to 400 °C (Mazzini et al.,
126　2012). Measurements reveal that Lusi represents one of the largest natural gas systems on Earth,
127　with CH_4 emissions up to 0.1 Tg/year and CO_2 release comparable to large volcanic systems
128　(Mazzini et al., 2021). High helium isotopic ratios, with mantle-derived signature, have been
129　measured from the gas collected at Lusi (R/Ra = 7) and are those measured at the fumaroles of the
130　neighboring volcanic complex (R/Ra = 7.3) (Mazzini et al., 2012; Inguaggiato et al., 2018; Sciarra
131　et al, 2018). Regional tomography studies reveal that the Lusi conduit is connected at 4.5 km depth
132　with the volcanic complex through a magmatic intrusion/hydrothermal fluids migration propagating
133　towards the NE of Java Island (Fallahi et al., 2017). In agreement with these evidences, studies
134　completed on clast erupted from the Lusi crater, reveal that they had been exposed to temperatures
135　>350 °C, inconsistent with the local geothermal gradient extrapolated to the apparent source depth
136　(Malvoisin et al., 2018; Zaputlyaeva et al., 2020).

137   Accordingly, for our modeling, we consider an additional heat source supplied by magmatic

138   intrusion and related hydrothermal fluid migration at depth supplementing the initial conductive

139   geothermal gradient of 42°C/km measured prior to the eruption (Mazzini et al., 2007). The model

140   does not include magma flow and dynamics, only the added heat source, assumed to be at a depth of

141   5.5 km. We investigate two scenarios, one with fluid temperature at 500°C, consistent with a linear

142   interpolation of the thermometry data obtained on clasts erupted at Lusi (Malvoisin et al. 2018;

143   Zaputlyaeva et al., 2020), and the second with fluid temperature of 1,000°C, that considers a non-

144   linear temperature evolution with depth. The surface temperature is set to 27°C (Svensen et al.,

145   2018). For rock properties, we used the parameters found in Svensen et al. (2018) for the lithology,

146   combined with analyses from Mazzini et al. (2012) and Tanikawa et al. (2010). We assume that the

147   flow properties of supercritical CO_2 are similar to those of water because supercritical CO_2 is ten

148   times more compressible than water, but it is also about ten times less viscous (Miller et al., 2004).

149   This allows modeling fluid flow by considering only one fluid phase, which is a valid assumption

150   for most of the modeling domain except near the surface where gas forms. This may have

151   consequences on temperature estimates at shallow depth because the latent heat of vaporization is

152   not incorporated in the heat conservation equation. Because we consider a one-phase H_2O-CO_2

153   mixture, mud transport is not simulated. Clay dehydration and mass and heat transport in porous

154   media are linked to porosity and permeability changes, which may affect outflow at the surface.

155   Dehydration reactions involve large and sometimes rapid volume changes related to free water

156   release from the clay mineralogical structure. They occur not only during diagenesis but also as a

157   result of pressure and temperature increase during metamorphism (Vidal and Dubacq, 2009). The

158   reaction of the two main clay layers (Upper Kalibeng Formation and Ngimgbang Formation)

159   (Figure 2b) may thus change the thermo-hydrodynamic properties of the sediment-hosted Lusi

160   system.

161

2.1 Physical model

163   The aim of our work is to model the impact of clay dehydration on the Lusi fluid flow. Modeling

164   the complex couplings between reaction, fluid flow and deformation is usually performed with pre-

165   existing codes (e.g. Xu et al., 2011). However, the achievable resolution using such models is low

166   (approximately several thousands of grid cells; Izadi and Elsworth, 2013; Shabani et al., 2020),

167   precluding the inclusion of complex geological structures. Fluid migration and flow at Lusi are

168   apparently controlled by the Watukosek Fault system (Mazzini et al., 2009) so that it is essential to

169   use at least moderately high-resolution. To attain such definition, the physical model is simplified in

170   an effort to highlight processes playing a first-order role on fluid flow at Lusi (dehydration, heating,

permeability evolution). The approach presented here does not use separate modules to implement reaction, fluid flow and deformation, and instead fully coupled fluid pressure and porosity variations are calculated in single equations (Malvoisin et al., 2015). We use a continuum porous media approach and solve the governing nonlinear equations with the Finite Difference (FD) method. Clay dehydration reactions can play a significant role in the evolution of porosity and permeability and may also contribute to over-pressure development. Production of fluid through dehydration reactions establishes pore pressure gradients that then must diffuse to the surroundings. Mazzini et al. (2007, 2018) measured lower salinity in the fluids expelled at Lusi than in seawater, and attributed this dilution to clay dehydration based on enrichment in B, Li and ^{18}O and a depletion in ^{2}H in the expelled fluids. Analyses on side well cores from the BJP1 borehole, located in the vicinity of Lusi, revealed that illite-smectite transformation (a dehydration reaction) occurs in the sediments of the Bluish Grey clays from the Upper Kalibeng Formation (Mazzini et al., 2007).

We model the temperature-dependent clay dehydration by fitting the water content/temperature curve found in Vidal & Dubacq (2009) for the illite-smectite transformation. We use the 3D geological model proposed by Sohrabi et al. (2018) to generate a distribution of porosity and permeability, and the 3D multi-GPU simulator developed by Sohrabi et al. (2019) for clay dehydration.

2.1.1 Mass conservation

We compute fluid pressure (*Pf*), temperature (*T*), porosity (ϕ) , permeability (*k*), and fluid generation from clay dehydration as follows.

Total mass conservation in a porous and reacting medium is:

$$\frac{\partial(\rho_f \phi + \rho_s(1 - \phi))}{\partial t} + \nabla \cdot \left(\rho_f \phi v_f + \rho_s(1 - \phi)v_s\right) = 0$$

(1)

where ϕ, ρ, v are the porosity (volume fraction of fluid), density and velocity, respectively, and subscripts 's' and 'f' denote the properties of the solid and the fluid. Mass of nonvolatile species is conserved by (Malvoisin et al., 2015):

$$\frac{\partial(\rho_s(1 - X_s)(1 - \phi))}{\partial t} + \nabla \cdot (\rho_s(1 - X_s)(1 - \phi)v_s) = 0$$

(2)

6

199 where the amount of fluid into the solid X_s is calculated at the equilibrium with a fit of the data of

200 Vidal and Dubacq (2009), which gives X_s as a function of temperature in the smectite/illite system.

201 **2.1.2 Conservation of momentum**

202 Conservation of fluid momentum is expressed by Darcy's law:

$$\phi(v_f - v_s) = -\frac{k_0 \phi^3}{\mu_f}(\nabla P_f - \rho_f g)$$

203 (3)

204 where the permeability (k) is related to the porosity through the Kozeny-Carman relationship with

205 an exponent 3 and a constant background permeability k_0 (Kozeny, 1927; Carmen, 1937; Carmen,

206 1956), μ_f is the fluid viscosity, g is the gravitational constant, and P_f is the fluid pressure.

207

208 The fluid pressure considering the effects of clay dehydration on volume change (rock density ρ_s

209 constant without viscous deformation) can be expressed as (Malvoisin et al., 2015):

210

$$\nabla \frac{k_0 \phi^3}{\mu_f}(\nabla P_f - \rho_f g) = \beta_{eff}\frac{dP_f}{dt} + \left(1 - \frac{\rho_s}{\rho_f}\right) \cdot \frac{1 - \phi}{1 - X_s} \cdot \frac{dX_s}{dt}$$

211 (4)

212 where the partial time derivatives are replaced by material derivatives ($\frac{d}{dt} = \frac{\partial}{\partial t} + \nabla v_s$) and β_f and

213 β_s are the fluid and pore (crack) compressibility. The effective compressibility β_{eff} is described by:

$$\beta_{eff} = \beta_f + \frac{\beta_s}{1 - \phi}$$

214 (5)

215 The hydro-mechanical porosity change due to fluid production by metamorphism can be expressed

216 by (Malvoisin et al., 2015):

217

$$\frac{d\phi}{dt} = \beta_s \frac{dP_f}{dt} - \frac{(1 - \phi)}{(1 - X_s)} \cdot \frac{dX_s}{dt}$$

218 (6)

219 **2.1.3 Energy conservation**

220 Energy heat conservation over an elemental volume of medium (solid and fluid phase) at thermal

221 equilibrium so that $T = T_s = T_f$ (Nield & Bejan, 2006) is:

7

$$\left((1-\phi)\rho_s c_s + \phi(\rho_f c_f)\right)\frac{\partial T}{\partial t} + (\rho_f c_f)v_f \cdot \nabla T$$

$$= \nabla \cdot \left(\left((1-\phi)\lambda_s + \phi\lambda_f\right)\nabla T\right) + \left((1-\phi)q_s + \phi q_f\right)$$

222   (7)

223 where c is the specific heat of the phase, λ is the thermal conductivity and q is the heat production

224 per unit volume. Equations 1 to 7 results in a highly nonlinear system of differential equation solved

225 here by using the Finite Deference (FD) method.

226 The general coupled parameters used for simulations are shown in Table 1. Parameter values chosen

227 for the fully coupled 3D numerical model (Table 1) are inputs measured and calculated from

228 previous studies.

229

Table 1: Parameters definition and values used.

Symbol	Definition	Parameters	Units
P_f	Fluid pressure	-	Pa
ρ_f	Density of fluid	-*	$kg \cdot m^{-3}$
ρ_s	Density of solid	2650	$kg \cdot m^{-3}$
v_f	Velocity of fluid	-	$m \cdot s^{-1}$
β_f	Compressibility of fluid	$1e^{-10}$	Pa^{-1}
β_s	Compressibility of solid	$1e^{-9}$	Pa^{-1}
β_{eff}	Effective Compressibility	-	Pa^{-1}
ϕ	Porosity	-	-
k	Permeability	-	m^2
X_s	Mass fraction of fluid in solid	-	wt %
T	Temperature	-	°C
c_f	Fluid specific heat	4190	$J/kg \cdot K$
c_s	Solid specific heat	1000	$J/kg \cdot K$
λ_f	Fluid thermal conductivity	0.6	$W/m \cdot K$
λ_s	Solid thermal conductivity	2.1	$W/m \cdot K$
q_f	Fluid heat production	-	$J/m^3/s$
q_s	Solid heat production	-	$J/m^3/s$
g	Gravity acceleration	9.81	$m^2 s^{-1}$

230

231   * calculated with the Equation of State (EOS) from Sun et al. (2008).

232

3. Results

We generated a numerical grid for multi-GPU computing from the 3D geological model (Figure 3). We performed 3D simulations in space and time to quantify the effects of clay dehydration in the Upper Kalibeng (purple) and the Ngimgbang (yellow) Formations. We numerically investigated two scenarios with different heated fluid temperatures (500°C and 1,000°C). Time zero was chosen as the onset of the fluid eruption in 2006. Figures 4 and 5 show the calculated parameters through the shear zones/faults as pressure (P_f), temperature (T), porosity (ϕ), permeability (k) and the quantity of fluid (X_s).

We simulated up to 200 years of the system evolution. However, we present only the first 50 years of simulation because fluids produced by dehydration are expected to mostly exhausted by this time. The temperature distributions for the two considered scenarios are different (Figure 4a and Figure 5a). We observe over pressure in the Upper Kalibeng clay Formation of up to 5-10 MPa (Figure 4b and Figure 5b). Through the 50 years of simulation, we perceive that the Ngimgbang and the Upper Kalibeng Formations liberate ~ 17 % and ~ 40 % of their stored water, respectively. This amount of water release modifies the porosity and the permeability of the shear zones/faults (Figure 4c, d and Figure 5c, d). Figure 4e and Figure 5e show that clay layers had already been largely dehydrated by diagenesis before Lusi started to erupt (e.g. illization, Mazzini et al., 2007).

Figure 6 and Figure 7 show the evolution of the temperature through the entire Lusi system. These calculated temperatures do not represent the fluid temperature at shallow depth, because two important shallow physical processes are not considered in this work. The latent heat of vaporization, as already discussed, is not implemented neither is the meteoritic and groundwater recharge in the system. Both these processes are extremely efficient in significantly dropping the fluid temperatures of the active system at shallow depths. Figure 8 and Figure 9 show the porosity through the two shear zones/faults (Watukosek and Siring faults) during 50 years of activity. We observe that the temperature of fluid source (500°C or 1,000°C) does not strongly modify the overall temperature distribution in the system over this time scale. The system comes to equilibrium after a certain time. The calculated porosity evolution shows that a 500°C fluid source generates less change in the rock properties of the Ngimgbang Formation than in the Upper Kalibeng Formation.

We computed the amount of fluid released from the two different clay layers (Upper Kalibeng and Ngimgbang Formation) after Lusi began to erupt (Figure 10). The Upper Kalibeng Formation re-leases four times (~ 4x) more water than the Ngimgbang Formation. Simulated results within the first decade overestimate by a factor of ~ 2 to 3 the measured outflow of fluids at the Lusi site (Mazzini et al., 2007; Mazzini et al., 2012). The simulated volume of water released is 240,000

9

267   m^3/day for a fluid source at 1,000°C and 230,000 m^3/day for fluids at 500°C during the first decade.

268   Simulated outflow caused by clay dehydration was around 60,000 m^3/day after 25 years and 343

269   m^3/day after 50 years for a fluid source at 1,000°C. Using instead 500°C, simulated water release

270   was around 51,000 m^3/day after 25 years and 184 m^3/day after 50 years. After 25 years, the tem-

271   perature in the conduit (Watukosek and Siring faults intersection) is constant at depths greater than

272   ~ 1,500 m (Figure 4a and Figure 5a). As a result, fluid production in the two clay layers ceases

273   (Figure 4e and Figure 5e).

274

4. Discussion

4.1 Hydrothermal system of Lusi: evolution and lifetime

277   We investigated the influence of a high-temperature intrusion/hydrothermal fluids migration at

278   depth on clay dehydration, using a high-resolution 3D numerical model. We integrate previous field

279   data measurements and calculations (Mazzini et al., 2007; Mazzini et al., 2012; Mazzini, 2018).

280   Results show that dehydration from two clay layers will continue to drive the Lusi system. The

281   model proposed here invokes clay dehydration after ascent of hot fluids from a deep source. This

282   process was suggested by geochemical measurements (Mazzini et al., 2007; Mazzini et al., 2012;

283   Malvoisin et al., 2018) and we demonstrate here that it can explain aqueous fluid ascent and

284   eruption at Lusi. Flow dynamics controlled by hot fluid ascent may partly reproduce a geyser

285   behaviour, even though the Lusi pulsations are not predicted here (Mazzini et al., 2007; Zoporowski

286   and Miller, 2009; Karyono et al., 2017; Lupi et al., 2018). Geysering is "almost" always associated

287   with multiphase flow. The fact that it does not occur in these simulations probably reflects, at least

288   in part, the single-phase approximation. The Lusi system is of potential resource interest on the long

289   term, regardless the initial temperature of the fluid source. The simulations show fluid flow mainly

290   controlled by the highly permeable pathways provided by fault/shear zones, and these could be

291   targeted for geothermal energy.

292   Model simulations show that dehydration of the underlying clay layers around ~ 1,500 m (Upper

293   Kalibeng Formation) and ~ 5,000 m (Ngimgbang Formation) could release additional fluid in the

294   future. We investigated two scenarios, and both overestimate by a factor of 2-3x fluid production

295   when compared with on-site measurements. However, these measurements only considered outflow

296   from the main vents (Mazzini et al., 2021) and do not include the large quantities of water released

297   from other active vents.

298   Our model considers one fluid phase and does not implement the latent heat of vaporization. It is

299   thus unable to model vaporization and its effect on temperature. After magma emplacement at

depth, the temperature progressively increases towards the surface up to values above 100°C after 10 years of simulated eruption (Figure 5). The lack of heat extraction due to vaporization also induces temperature overestimation at depth after 10 years of simulated eruption. This effect is more pronounced near the surface, that is in the Upper Kalibeng Formation rather than in the Ngimgbang Formation. The main objective of our model is to investigate the effect of clay dehydration on fluid dynamics at Lusi. Dehydration is complete in the Ngimgbang Formation in the first 10 years of the eruption. Two thirds of the maximum dehydration and of the porosity increase also occur in the Upper Kalibeng Formation during this period (Figure 5c and Figure 5e). Neglecting vaporization in our model thus only affects one third of the predicted dehydration after 10 years of eruption in the Upper Kalibeng Formation. Vaporization will induce cooler temperature in this formation than predicted with the model. This will slow down its dehydration. The duration of the eruption of 50 years predicted here is thus a minimum. The amount of liberated fluid could also be overestimated by a maximum of one third since vaporization could also reduce the maximum temperature reached in the Upper Kalibeng Formation during the eruption.

Water liberation through dehydration calculated here depends in part on the uncertainties associated with the 3D geological model. Further, the physics applied here do not consider the effect of reaction on heat budget (Eqs. 1 to 7), the influence of boiling, or possible cooling by meteoric water. This explains why the results found in Figure 4a and Figure 5a greatly overestimate shallow temperature in the shear zones/faults zone at later simulation times. The overly high simulated temperatures may also explain why the extent of dehydration in the Upper Kalibeng Formation is 15% higher in the model (82% of dehydration) than in the natural samples (65% illitization; Mazzini et al., 2007). Groundwater recharge from the sediment-hosted system and fluid flow in the shallow surface linked to the Arjuno-Welirang volcanic complex should also be considered in future simulations, to encompass the hydrogeological complexity of the region.

This is the first 3D computational model of the Lusi's mud eruption that estimates the contribution of clay dehydration to fluid generation at depth (Figure 11). However, it considers single-phase flow of an aqueous fluid. This approximation is justified at depth greater than ~ 1,800 m, since large part of the mud is believed to originate in the Upper Kalibeng Formation (Mazzini et al., 2007). As mud is more viscous than pure aqueous fluid, this may lead to overestimation of fluid velocity in the top part of our model. Zoporowski and Miller (2009), Rudolph et al. (2011) and Collignon et al. (2018) investigated mud flow between the mud source and the surface with single-phase, two-dimensional models considering mud as a viscous fluid. However, the impact of interplay between the various phases is still poorly constrained. This hampers our ability to accurately predict flow dynamics, especially near the surface where mud and aqueous fluid coexist and gas can form. Developing a

multi-phase numerical model of Lusi should thus be targeted for future numerical investigation. Further, even though our model provides more complete treatment of the geological complexity at Lusi, it does not solve for stress evolution. We consider the influence of the Watukosek Fault System on permeability but do not model fluidization and subsidence associated with faulting, which is known to play a key role on fluid dynamics at Lusi (Istadi et al., 2009; Mazzini et al., 2009; Osorio et al., 2021). Finally, other processes may deserve to be considered for in future large-scale numerical modeling; including thermal maturation of organic matter in contact with a magmatic intrusion at depth (Svensen et al., 2018), and focusing of seismic waves, which may favor fluidization (Lupi et al., 2013; Lupi et al., 2014).

If, in the future, we see a notable increase of the geothermal gradient across the entire sediment-hosted hydrothermal system of East Java, we will have to recalculate and re-estimate the initial conditions invoked in our simulations. In addition, if the fluid outflow at the Lusi site does not decrease on a decadal scale, we might infer that the fluid discharging from the Lusi vent is recharged by other sources.

4.2 Implications for potential geothermal resources

Hydrothermal systems can be found in many places and used as geothermal energy resources, as in Italy (e.g. Lardarello), Iceland (e.g. Blue Lagoon), and the U.S.A. (e.g. The Geysers). Each of these systems has a specific hydrogeological environment and its own complexity. At Lusi dehydration may be an important element. The Salton Sea (California, U.S.A.), a sediment-hosted hydrothermal system (Svensen et al., 2007; Mazzini et al., 2011), may bear some resemblance to Lusi (Mazzini et al., 2018). However, Salton Sea system has been geologically active for a long while compared to Lusi. There, deep heated fluids fill the system and structural clay dehydration causes porosity evolution at a different scale. Our results show that for 50 years following the Lusi inception in 2006, the dynamics and thermodynamics will be strongly dependent on this process, which induces irreversible physical changes to the rock via water release.

Our high-resolution 3D numerical simulations track the controlled rock property changes (dehydration) over 50 years. The models suggest that the clay dehydration should decrease after 25 years and may stop after 50 years. The complex volcanic structure in the vicinity of Lusi is a potential source of geothermal energy for the surrounding population as reflected by the simulation distribution of temperature in time and space (Figure 6 and Figure 7). The simulations suggest evolving property profiles which may control hydro-thermo-mechanical structure over time.

5. Conclusions

We present 3D numerical simulations using multi-GPU computing of fluid thermo-hydrodynamics with porosity and permeability evolution driven by hydrothermal fluid intrusion at 5.5 km depth below the active Lusi eruption. Starting from 2006, the results demonstrate that Lusi decreasing less outflow due to decreasing clay dehydration (in the Upper Kalibeng Formation and Ngimgbang Formation) over the next decade. Our simulations suggest that the contribution of dehydration to water release may essentially stop after 25 years of activity and completely stop after 50 years.

Clay mineral illitization, already ongoing before the eruption, continues mainly in the Upper Kalibeng Formation but also in the Ngimgbang Formation under conditions of increasing temperature and pressure. This process is irreversible and may be complete after about 50 years. The simulations are consistent with the degree of illitization measured on site. Heating of the Upper Kalibeng Formation could produce hydro-fractures which will enhance a preferential pathway for fluid to the surface. Porosity and permeability evolution in time can have a non-negligible effect.

The Lusi activity may still persist after 50 years because of the groundwater recharge of the entire hydrothermal system linked to the Arjuno-Welirang volcanic complex.

The initial temperature of the source fluids (500°C or 1,000°C) does not have a significant influence on the entire system. Temperatures are better reproduced during the first decade of Lusi activity with a hypothetic source at 500°C. The 10 MPa calculated overpressure calculated and the heated fluids coming from 5.5 km are primary controls on the clay dehydration rates.

3D numerical modeling can inform decision making on natural or engineered systems. High-Performance Computing (HPC) is a valuable technique to model physical processes in a reasonable computational time. Geothermal reservoir valorization is an important topic today. Decisions have to be made regarding use of renewable energy. Deeper boreholes and complementary coupled numerical physical analyses are needed to evaluate this potentially large geothermal energy supply.

Data availability

The relevant data to reproduce the numerical results are provided in the manuscript. The remaining data used in this study are available from cited references. All data and materials that support the findings of this study can be made available, in some form, to any researcher for purposes of reproducing or extending the analysis upon reasonable request to the corresponding author R.S.

Code availability

The numerical code used in this study is available from cited reference (with restrictions) upon reasonable request.

Figure captions

417 **Figure 1**: a) Inset map of Indonesia and topographic map showing the Arjuno-Welirang volcanic

418 complex to the south with some of the surrounding hydrothermal springs. Lusi and other mud

419 volcanoes are located to the north of the island inside the sedimentary basin. b) Aerial image

420 showing erupting craters in the central part of the inaccessible hydrothermal pond.

421

422 **Figure 2**: Conceptual model for fluid pressure increase controlled by dehydration in a deep

423 hydrothermal system or geothermal reservoir. Under conditions of increasing temperature and

424 pressure, clay dehydration reactions begin. a) 3D conceptual model considering five main

425 stratigraphic units and two main shear zone/faults at Lusi site. b) 3D model set-up for simulations,

426 considering deep heated fluids filling the entire Lusi hydrothermal system.

427

428 **Figure 3**: 3D structural numerical grid with initial parameters permeability (k) and porosity (ϕ)

429 distribution at high-resolution (384x384x384) for multi-GPU calculation. This numerical grid is

430 based on the 3D geological model of Lusi presented in Sohrabi et al. (2018).

431

432 **Figure 4**: Evolution of simulated a) temperature, b) pressure, c) porosity, d) permeability and e)

433 water liberation through the Lusi shear zones/faults after fluid intrusion at 500°C after: 0 years

434 (red), 5 years (green), 10 years (blue), 25 years (magenta) and 50 years (dashed cyan).

435

436 **Figure 5**: Evolution of simulated a) temperature, b) pressure, c) porosity, d) permeability and e)

437 water liberation through the Lusi shear zones/faults after fluid intrusion at 1,000°C after: 0 years

438 (red), 5 years (green), 10 years (blue), 25 years (magenta) and 50 years (dashed cyan).

439

440 **Figure 6**: Evolution of temperature from an initial geothermal gradient of 42°C/km throughout the

441 system and fluid intrusion at 500°C with input parameters presented in the 3D geological model

442 (Figure 3). Times are since Lusi erupted.

443

444 **Figure 7**: Evolution of temperature from an initial geothermal gradient of 42°C/km throughout the

445 system and fluid intrusion at 1,000°C with input parameters presented in the 3D geological model

446 (Figure 3). Times are since Lusi erupted.

447 **Figure 8**: Evolution of porosity after fluid intrusion at 500°C with input parameters presented in the

448 3D geological model (Figure 3). The two shear zones/faults are shown with a focus on the two clay

449 layers (Upper Kalibeng Formation and Ngimgbang Formation). Times are since Lusi erupted.

450

Figure 9: Evolution of porosity after fluid intrusion at 1,000°C with input parameters presented in the 3D geological model (Figure 3). The two shear zones/faults are shown with a focus on the two clay layers (Upper Kalibeng Formation and Ngimgbang Formation). Times are since Lusi erupted.

454

Figure 10: Release water due to the dehydration of the two main clay layers over 50 years after Lusi started to erupt in 2006. The red line shows results for the fluid intrusion at 1,000 °C and the blue line results for fluid intrusion at 500 °C. The green circles are outflow data measured at the Lusi vent.

459

Figure 11: Conceptual model based on the numerical simulations performed in this work. Heated fluids associated with magmatic intrusion at depth induces clay dehydration feeding the Lusi mud eruption.

References

Bangerth, W., Hartmann, R., Kanschat, G. (2007). Deal. II-a general purpose object-oriented finite element library. ACM transactions on Mathematical Software (TOMS). 33(4), 24

Bowen, Robert. (1979). Geothermal resources. London: New York: Applied Science Publishers; Halsted Press

Carman, P. C. (1937). Fluid flow through granular beds. Transactions-Institution of Chemical Engineeres, 15, 150-166.

Carman, P. C. (1956). Flow of gases through porous media. Academic press.

Collignon, M., Schmid, D. W., Galerne, C., Lupi, M., & Mazzini, A. (2018). Modelling fluid flow in clastic eruptions: Application to the Lusi mud eruption. Marine and Petroleum Geology, 90, 173-190.

Davies, R. J., Mathias, S. A., Swarbrick, R. E., & Tingay, M. J. (2011). Probabilistic longevity estimate for the LUSI mud volcano, East Java. Journal of the Geological Society, 168(2), 517-523.

Fallahi, M. J., Obermann, A., Lupi, M., Karyono, K., & Mazzini, A. (2017). The plumbing system feeding the Lusi eruption revealed by ambient noise tomography. Journal of Geophysical Research: Solid Earth, 122(10), 8200-8213.

Flemisch, B., Darcis, M., Erbertseder, K., Faigle, B., Lauser, A., Mosthaf, K., Müthing, S., Nuske, P., Tatomir, A., Wolff, M., Helmig, R. (2011). DuMux: DUNE for multi-{phase,component,scale, physics,…} flow and transport in porous media. Adv. Water Resour. 34(9), 1102–1112

Gaston, D., Newman, C., Hansen, G., Lebrun-Grandie, D. (2009). MOOSE: a parallel computational framework for coupled systems of nonlinear equations. Nucl. Eng. Des. 239(10), 1768–1778

Hammond, G.E., Lichtner, P.C., Mills, R.T. (2014). Evaluating the performance of parallel subsurface simulators: an illustrative example with PFLOTRAN. Water Resour. Res. 50(1), 208–228

497

498 Hurwitz, S., & Manga, M. (2017). The fascinating and complex dynamics of geyser
499 eruptions. Annual Review of Earth and Planetary Sciences, 45, 31-59.

500 Inguaggiato, S., Mazzini, A., Vita, F., & Sciarra, A. (2018). The Arjuno-Welirang Volcanic Complex
501 and the connected Lusi system: geochemical evidences. Marine and Petroleum Geology, 90, 67-76.

502

503 Ingebritsen, S. E., & Sanford, W. E. (1999). Groundwater in geologic processes. Cambridge
504 University Press.

505

506 Ingebritsen, S. E., Geiger, S., Hurwitz, S., & Driesner, T. (2010). Numerical simulation of magmatic
507 hydrothermal systems. Reviews of Geophysics, 48(1).

508

509 Istadi, B. P., Pramono, G. H., Sumintadireja, P., & Alam, S. (2009). Modeling study of growth and
510 potential geohazard for LUSI mud volcano: East Java, Indonesia. Marine and Petroleum
511 Geology, 26(9), 1724-1739.

512

513 Izadi, G., & Elsworth, D. (2013). The effects of thermal stress and fluid pressure on induced
514 seismicity during stimulation to production within fractured reservoirs. Terra Nova, 25(5), 374-380.

515

516 Jeanne, P., Rutqvist, J., Vasco, D., Garcia, J., Dobson, P. F., Walters, M., & Borgia, A. (2014). A 3D
517 hydrogeological and geomechanical model of an Enhanced Geothermal System at The Geysers,
518 California. Geothermics, 51, 240-252.

519

520 Karyono, K., Obermann, A., Lupi, M., Masturyono, M., Hadi, S., Syafri, I., Abdurrokhim, A., &
521 Mazzini, A., (2017). Lusi, a clastic-dominated geysering system in Indonesia recently explored by
522 surface and subsurface observations: Terra Nova, v. 29, p. 13-19

523

524 Kolditz, O., Bauer, S., Bilke, L., Böttcher, N., Delfs, J.O., Fischer, T., et al. (2012). OpenGeoSys: an
525 open source initiative for numerical simulation of thermo-hydro-mechanical/chemical (THM/C)
526 processes in porous media. Environ. Earth Sci. 67(2), 589–599

527

528 Kozeny, J. (1927). Uber kapillare leitung der wasser in boden. Royal Academy of Science, Vienna,
529 Proc. Class I, 136, 271-306.

530

531 Lichtner, P.C., Carey, J.W. (2006). Incorporating solid solutions in reactive transport equations
532 using a kinetic discrete-composition approach. Geochimica et Cosmochimica Acta. 70(6), 1356–
533 1378

535 Lichtner, P.C., Kang, Q. (2007). Upscaling pore-scale reactive transport equations using a
536 multiscale
537 continuum formulation. Water Resources Research. 43, W12S15

539 Lowenstern, J. B., & Hurwitz, S. (2008). Monitoring a supervolcano in repose: Heat and volatile
540 flux at the Yellowstone Caldera. Elements, 4(1), 35-40.

542 Lupi, M., Saenger, E., Fuchs, F., Miller S.A. (2013). Lusi mud eruption triggered by geometric
543 focusing of seismic waves. Nature Geoscience, 6, 642–646.

545 Lupi, M., Saenger, E. H., Fuchs, F., & Miller, S. A. (2014). Correction: Corrigendum: Lusi mud
546 eruption triggered by geometric focusing of seismic waves. Nature Geoscience, 7(9), 687-688.

548 Lupi, M., Mazzini, A., Sciarra, A., Collignon, M., Schmid, D. W., Husein, A., ... & Karyono, K.
549 (2018). Enhanced hydrothermal processes at the new-born Lusi eruptive system, Indonesia. Journal
550 of Volcanology and Geothermal Research, 366, 47-57.

552 Malvoisin, B., Podladchikov, Y. Y., & Vrijmoed, J. C. (2015). Coupling changes in densities and
553 porosity to fluid pressure variations in reactive porous fluid flow: Local thermodynamic
554 equilibrium. Geochemistry, Geophysics, Geosystems, 16(12), 4362-4387.

556 Malvoisin, B., Mazzini, A., & Miller, S. A. (2018). Deep hydrothermal activity driving the Lusi
557 mud eruption. Earth and Planetary Science Letters, 497, 42-49.

559 Mazzini, A., Svensen, H., Akhmanov, G. G., Aloisi, G., Planke, S., Malthe-Sørenssen, A., & Istadi,
560 B. (2007). Triggering and dynamic evolution of the LUSI mud volcano, Indonesia. Earth and
561 Planetary Science Letters, 261(3), 375-388.

563 Mazzini, A., Nermoen, A., Krotkiewski, M., Podladchikov, Y., Planke, S., & Svensen, H. (2009).
564 Strike-slip faulting as a trigger mechanism for overpressure release through piercement structures.

Implications for the Lusi mud volcano, Indonesia. Marine and Petroleum Geology, 26(9), 1751-1765.

Mazzini, A., Svensen, H., Etiope, G., Onderdonk, N., & Banks, D. (2011). Fluid origin, gas fluxes and plumbing system in the sediment-hosted Salton Sea Geothermal System (California, USA). Journal of Volcanology and Geothermal Research, 205(3-4), 67-83.

Mazzini, A., Etiope, G., & Svensen, H., (2012). A new hydrothermal scenario for the 2006 Lusi eruption, Indonesia. Insights from gas geochemistry: Earth and Planetary Science Letters, v. 317-318, p. 305-318.

Mazzini, A. (2018). 10 years of Lusi eruption: Lessons learned from multidisciplinary studies (LUSI LAB).

Mazzini, A., Scholz, F., Svensen, H. H., Hensen, C., & Hadi, S. (2018). The geochemistry and origin of the hydrothermal water erupted at Lusi, Indonesia. Marine and Petroleum Geology, 90, 52-66.

Mazzini, A., Sciarra, A., Etiope, G., Sadavarte, P., Houweling, S., Pandey, S., and Husein, A. (2021). Relevant methane emission to the atmosphere from a geological gas manifestation: Scientific Reports, v. 11, no. 1, p. 4138.

Miller, S. A., Collettini, C., Chiaraluce, L., Cocco, M., Barchi, M., & Kaus, B. J. (2004). Aftershocks driven by a high-pressure CO_2 source at depth. Nature, 427(6976), 724.

Miller, S. A. & Mazzini, A. (2018). More than ten years of Lusi: A review of facts, coincidences, and past and future studies. Marine and Petroleum Geology, 90, 10-25.

Moscariello, A., Do Couto, D., Mondino, F., Booth, J., Lupi, M., & Mazzini, A. (2018). Genesis and evolution of the Watukosek fault system in the Lusi area (East Java). Marine and Petroleum Geology, 90, 125-137.

Nield, D. A. & Bejan, A. (2006). Convection in porous media (Vol. 3). New York: springer.

Obermann, A., Karyono, K., Diehl, T., Lupi, M., and Mazzini, A. (2018). Seismicity at Lusi and the adjacent volcanic complex, Java, Indonesia: Marine and Petroleum Geology, v. 90, p. 149-156.

Richards, J. R. (2011). Report into the past, present, and future social impacts of Lumpur Sidoarjo. Humanitus Sidoarjo Fund.

Osorio Riffo, Á., Mauri, G., Mazzini, A., and Miller, S. A. (2021). Tectonic insight and 3-D modelling of the Lusi (Java, Indonesia) mud edifice through gravity analyses: Geophysical Journal International, v. 225, no. 2, p. 984-997.

Rudolph, M. L., Karlstrom, L., & Manga, M. (2011). A prediction of the longevity of the Lusi mud eruption, Indonesia. Earth and Planetary Science Letters, 308(1-2), 124-130.

Samankassou, E., Mazzini, A., Chiaradia, M., Spezzaferri, S., Moscariello, A., & Do Couto, D. (2018). Origin and age of carbonate clasts from the Lusi eruption, Java, Indonesia. Marine and Petroleum Geology, 90, 138-148.

Sciarra, A., Mazzini, A., Inguaggiato, S., Vita, F., Lupi, M., & Hadi, S. (2018). Radon and carbon gas anomalies along the Watukosek fault system and Lusi mud eruption, Indonesia. Marine and Petroleum Geology, 90, 77-90.

Shabani, B., Pashin, J., & Vilcáez, J. (2020). TOUGHREACT-CO2 Bio–A new module to simulate geological carbon storage under biotic conditions (Part 2): The bio-geochemical reactive transport of CO2-CH4-H2-H2S gas mixtures. Journal of Natural Gas Science and Engineering, 76, 103190.

Sohrabi, R., Jansen, G., Malvoisin, B., Mazzini, A., & Miller, S. A. (2018). Numerical modeling of the Lusi hydrothermal system: Initial results and future challenges. Marine and Petroleum Geology, 90, 191-200.

Sohrabi, R., Omlin, S., & Miller, S. A. (2019). GEYSER: 3D thermo-hydrodynamic reactive transport numerical simulator including porosity and permeability evolution using GPU clusters. Computational Geosciences, 23, 1317-1330.

Steefel, C.I., DePaolo, D.J., Lichtner, P.C. (2005). Reactive transport modelling: an essential tool and a new research approach for the earth sciences. Earth Planet. Sci. Lett. 240(3–4), 539–558

634 Su, D., Mayer, K.U., MacQuarrie, K.T. (2017). Parallelization of MIN3PTHCm: a high-
635 performance computational framework for subsurface flow and reactive transport simulation.
636 Environ. Model Softw. 95, 271–289

638 Sun, H., Feistel, R., Koch, M., Markoe, A. (2008). New equations for density, entropy, heat
639 capacity, and potential temperature of a saline thermal fluid. Deep-Sea Res. I Oceanogr. Res. Pap.
640 55(10), 1304 - 1310.

642 Svensen, H., Karlsen, D. A., Sturz, A., Backer-Owe, K., Banks, D. A., & Planke, S. (2007).
643 Processes controlling water and hydrocarbon composition in seeps from the Salton Sea geothermal
644 system, California, USA. Geology, 35(1), 85-88.

646 Svensen, H. H., Iyer, K., Schmid, D. W., & Mazzini, A. (2018). Modelling of gas generation
647 following emplacement of an igneous sill below LUSI, east Java, Indonesia. Marine and Petroleum
648 Geology, 90, 201-208.

650 Tanikawa, W., Sakaguchi, M., Wibowo, H. T., Shimamoto, T., & Tadai, O. (2010). Fluid transport
651 properties and estimation of overpressure at the Lusi mud volcano, East Java Basin. Engineering
652 Geology, 116(1), 73-85.

654 Van Noorden, R. (2006). Mud volcano floods Java. Nature.

656 Vidal, O., & Dubacq, B. (2009). Thermodynamic modelling of clay dehydration, stability and
657 compositional evolution with temperature, pressure and H2O activity. Geochimica et
658 Cosmochimica Acta, 73(21), 6544-6564.

660 White, D. E. (1957). Thermal waters of volcanic origin. Geological Society of America
661 Bulletin, 68(12), 1637-1658.

663 White, M.D., Oostrom, M. (2003). STOMP subsurface transport overmultiple phases version 3.0
664 user's guide (No. PNNL-14286). Pacific Northwest National Lab., Richland, WA

666 Xu, T., Spycher, N., Sonnenthal, E., Zhang, G., Zheng, L., & Pruess, K. (2011). TOUGHREACT
667 Version 2.0: A simulator for subsurface reactive transport under non-isothermal multiphase flow
668 conditions. Computers & Geosciences, 37(6), 763-774.

669

670 Zhang, K.,Wu,Y.S., Pruess, K. (2008). User's guide for TOUGH2-MP- a massively parallel version
671 of the TOUGH2 code (No. LBNL– 315E). Ernest Orlando Lawrence Berkeley National Laboratory
672 Zaputlyaeva, A., Mazzini, A., Blumenberg, M., Scheeder, G., Kürschner, W. M., Kus, J., T.J.
673 Morgan & Frieling, J. (2020). Recent magmatism drives hydrocarbon generation in north-east Java,
674 indonesia. Scientific reports, 10(1), 1-14.

675

676 Zoporowski, A. & Miller, S. A. (2009). Modelling eruption cycles and decay of mud
677 volcanoes. Marine and Petroleum Geology, 26(9), 1879-1887.

Figure 1

a)

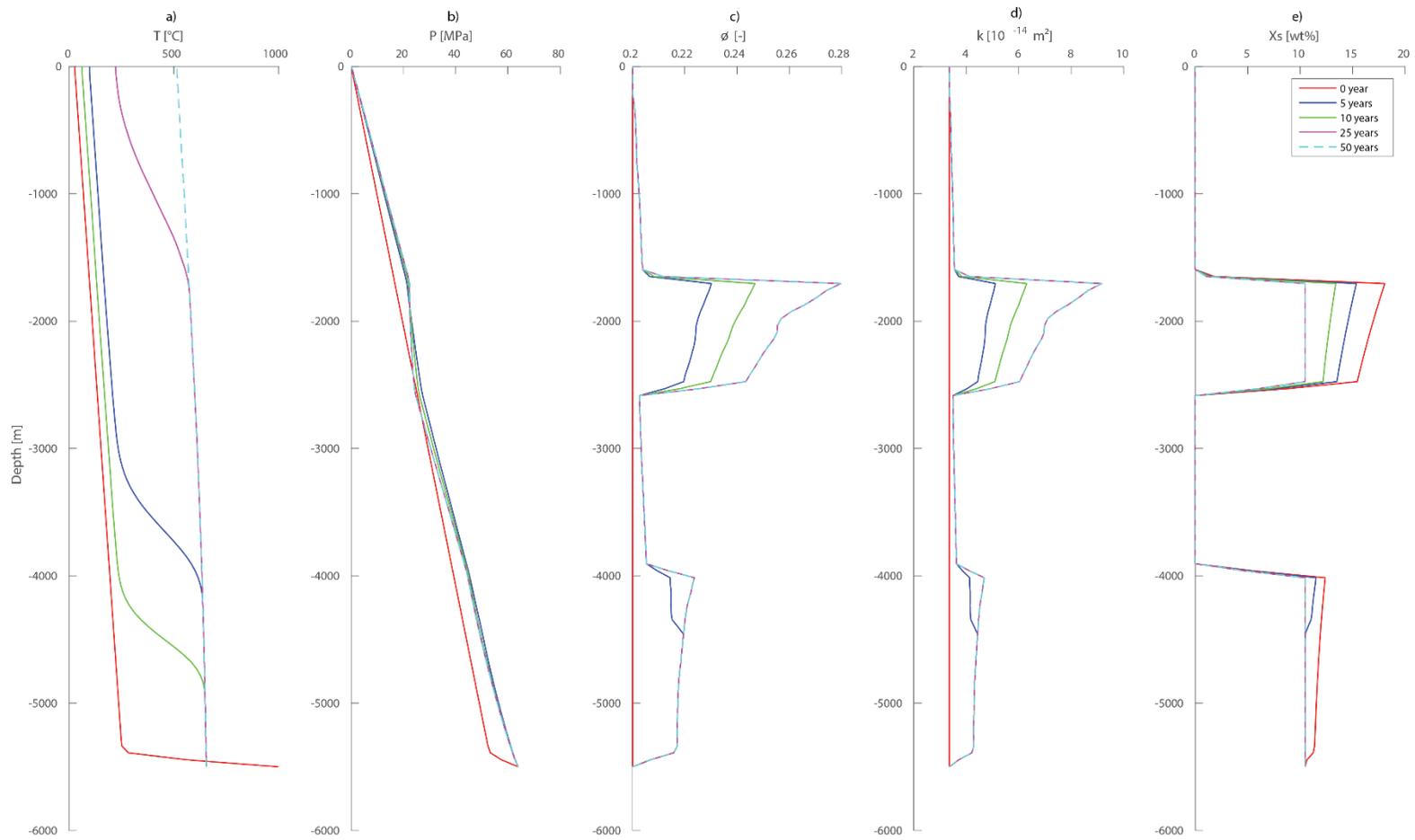SW   σ₁   NE

                        B

              A

Alt. Sand & Shales

~1500 m

Clay (mud layer)

σ₃   ~2500 m   σ₃

Volcanoclastics

~3000 m

Carbonate

~4000 m

Mudstone

~5500 m

σ₁

A: Watukosek Fault

B: Siring Fault

b)

Water + CO_2 + Dehydrated Rock

No flow

Open top, fixed atmospheric pressure,
fixed recharge temperature (27°C)

No flow

Upper Kalibeng Formation

Geothermal gradient (42°C /km)

Ngimgbang Formation

500°C or 1000°C

Heated fluids (Water + CO_2)
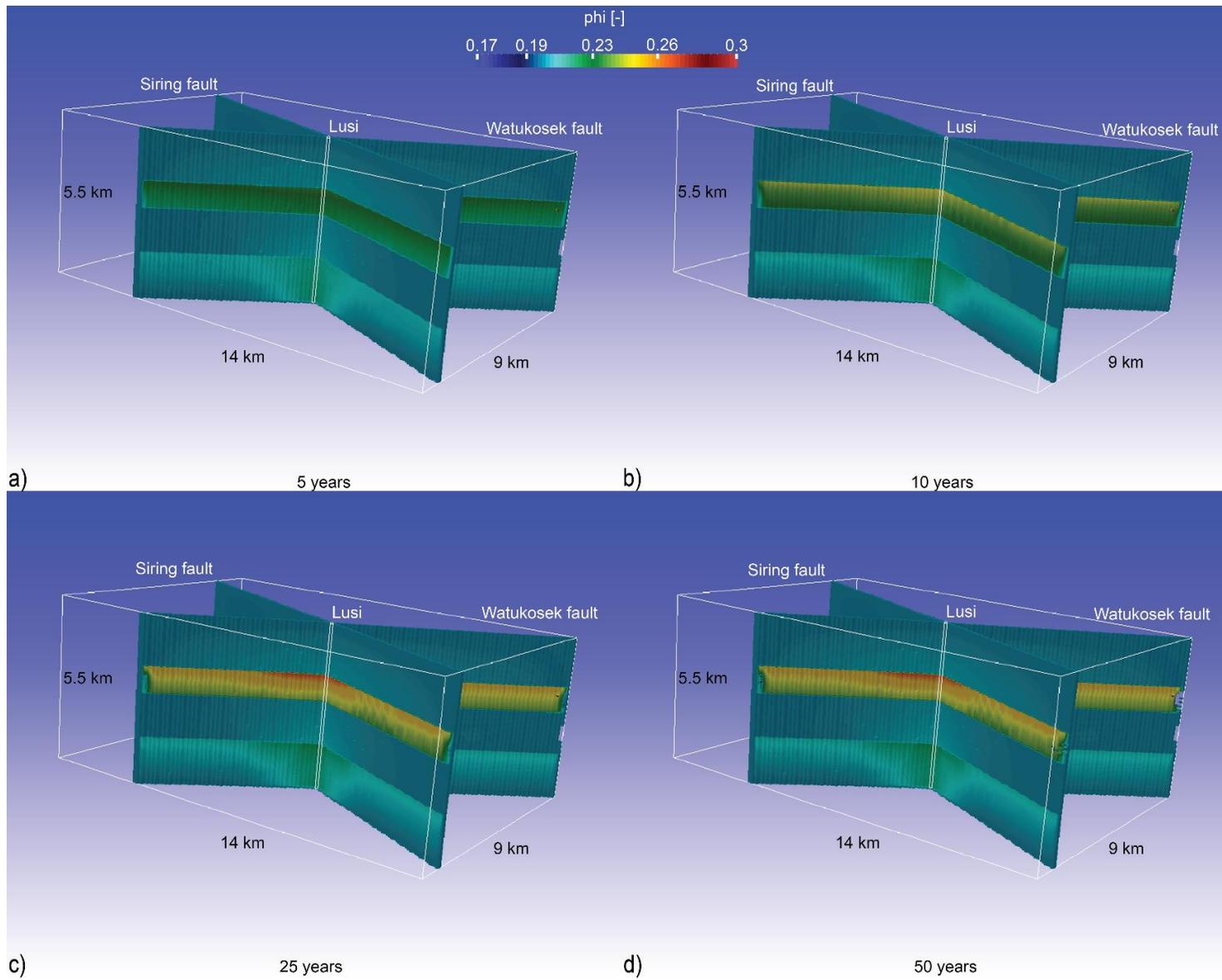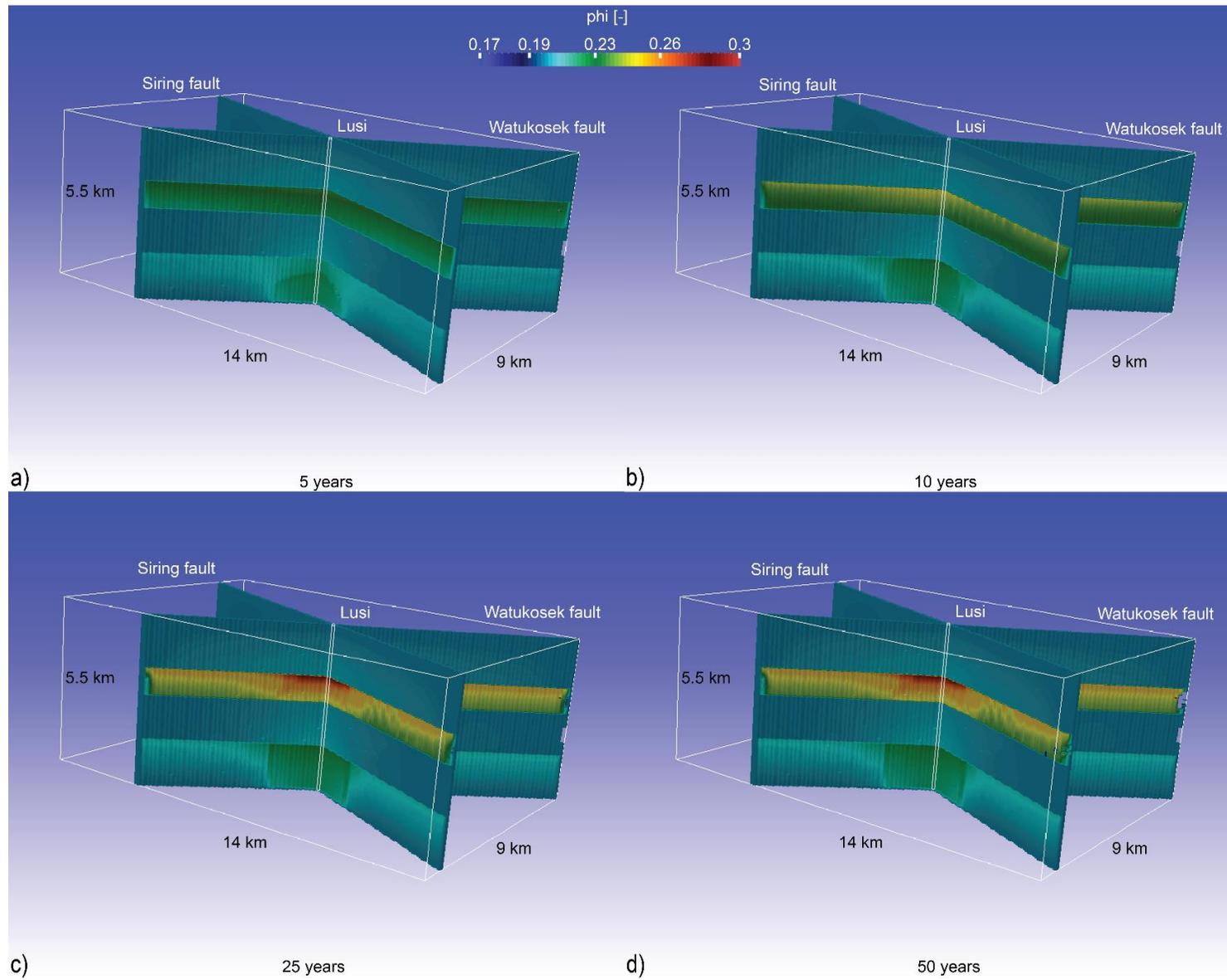
Figure 2

Figure 3

685

Figure 4

27

Figure 5

28
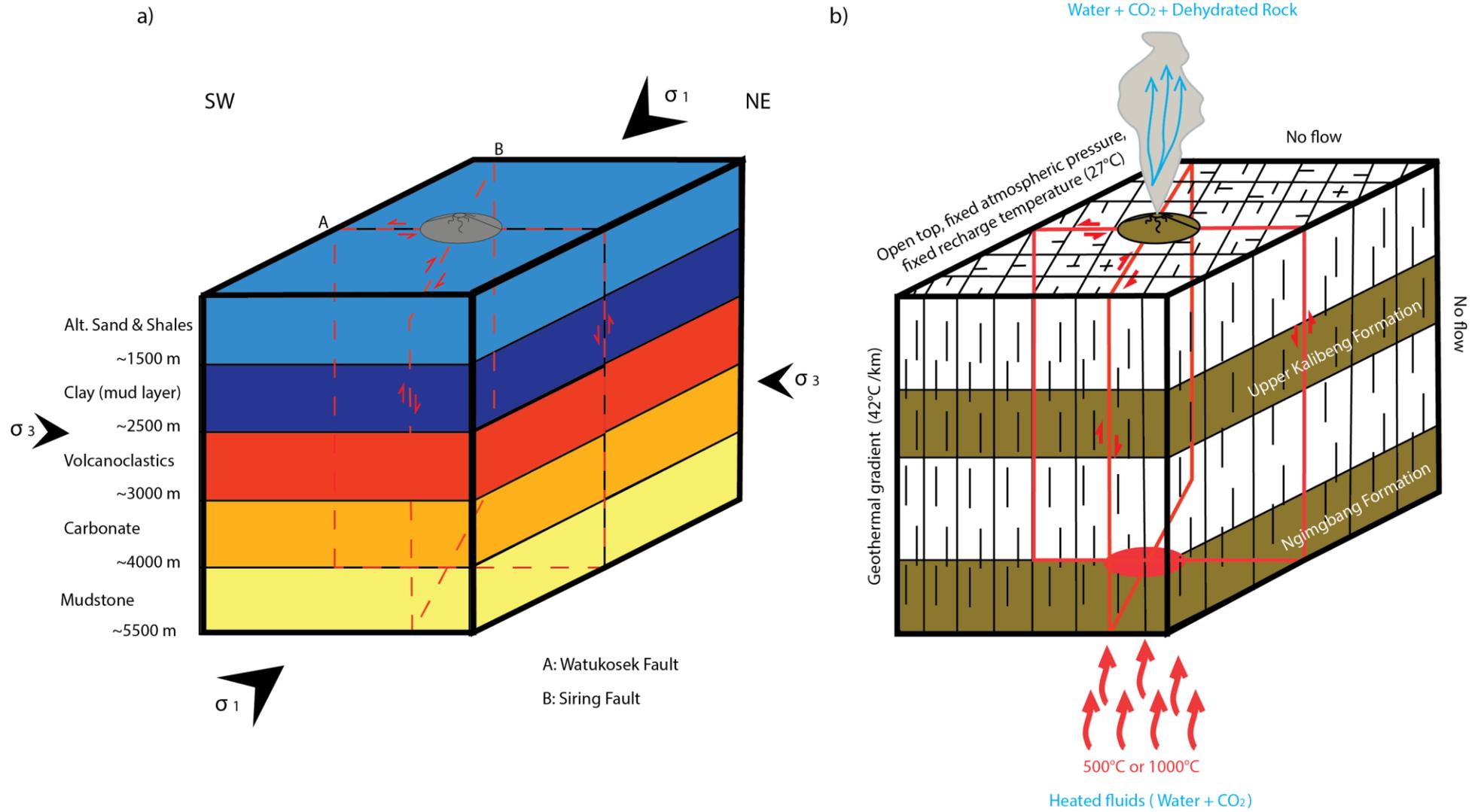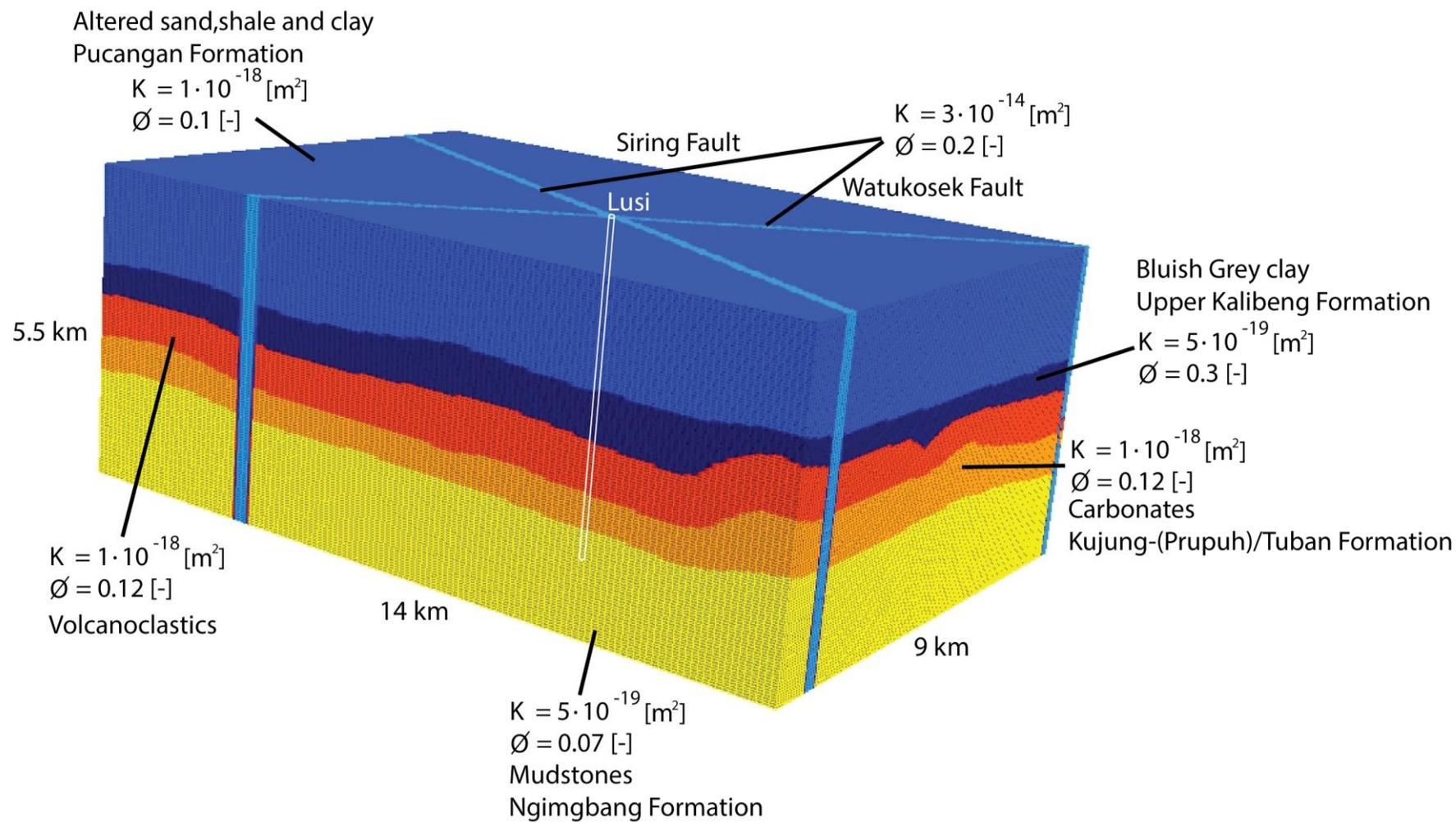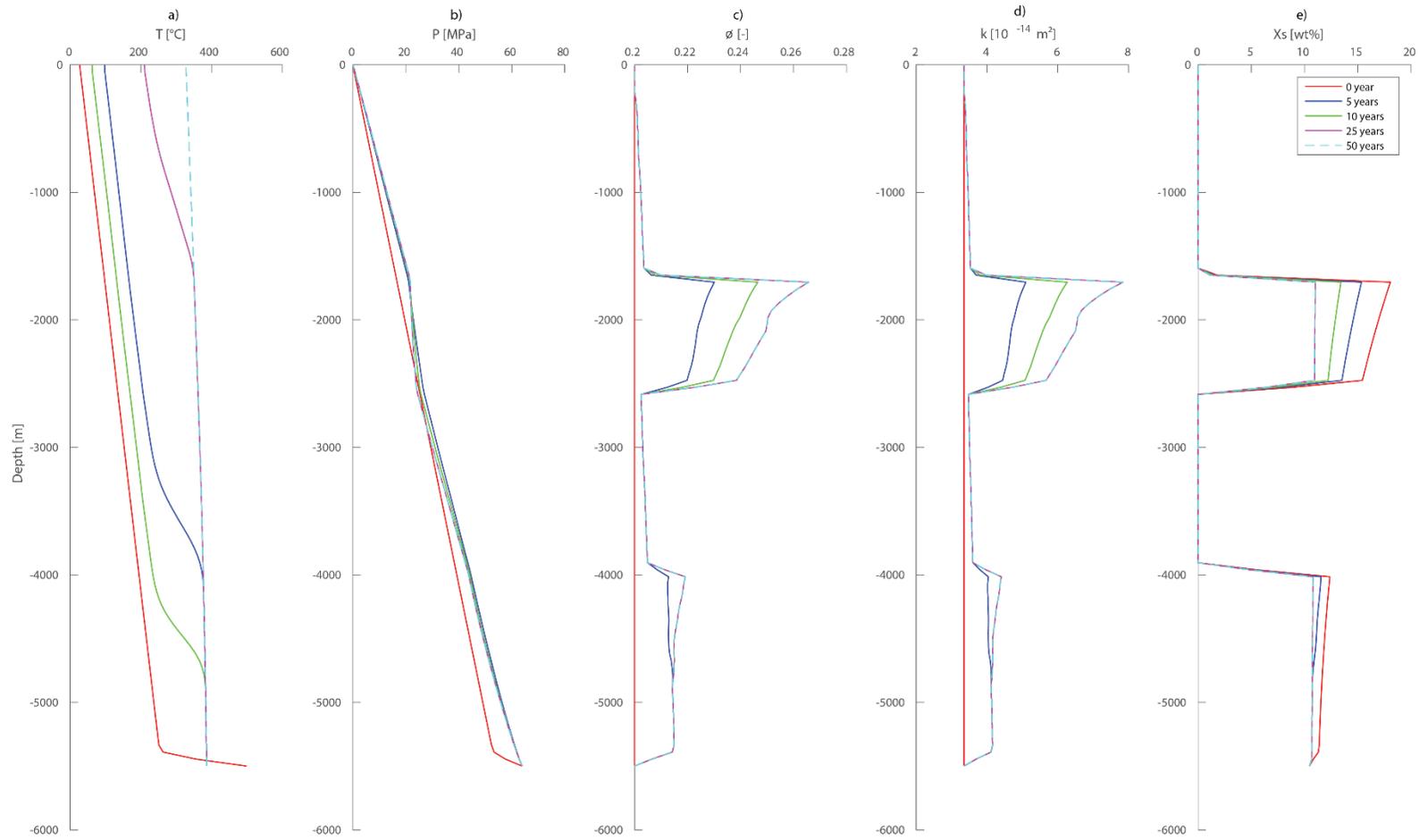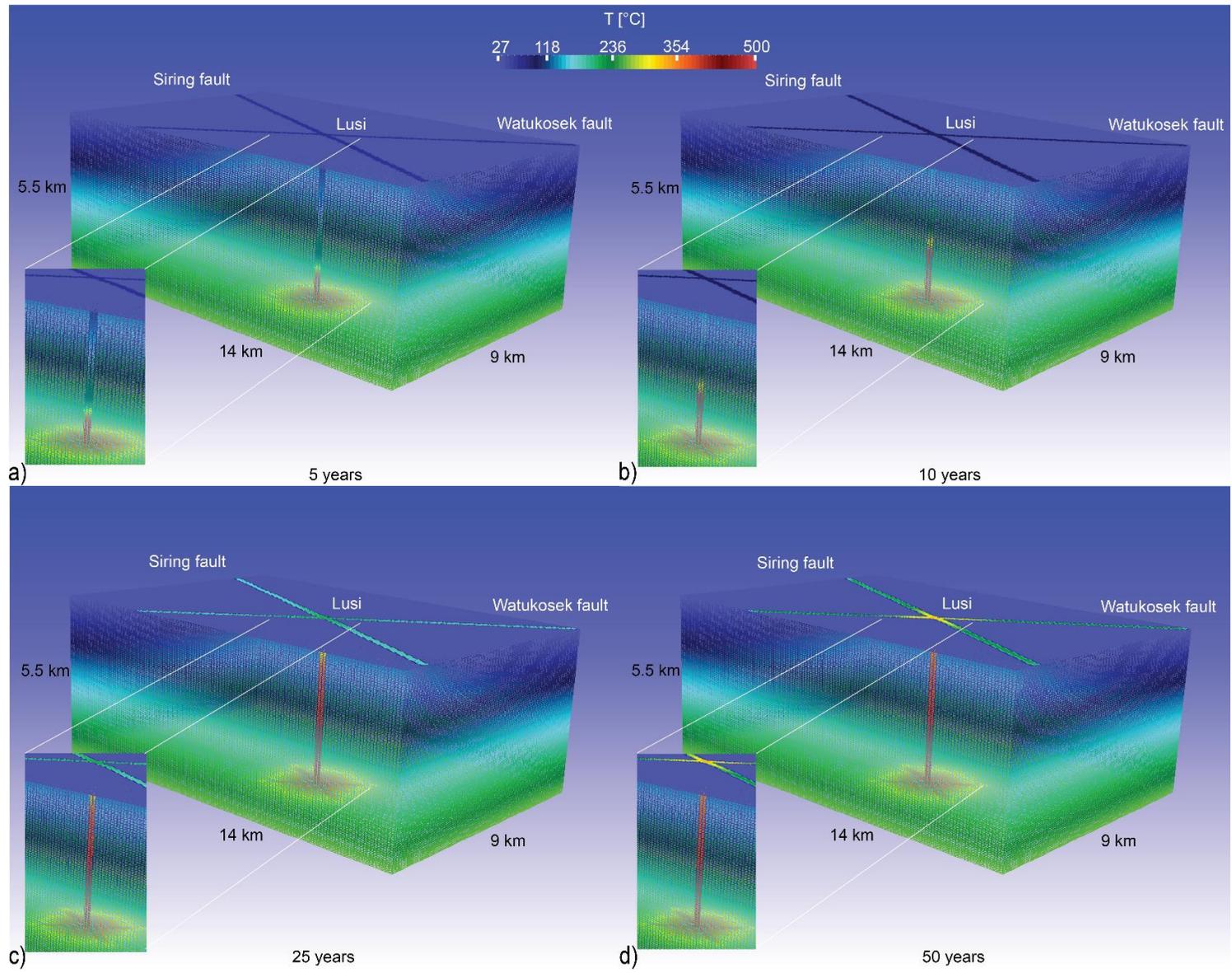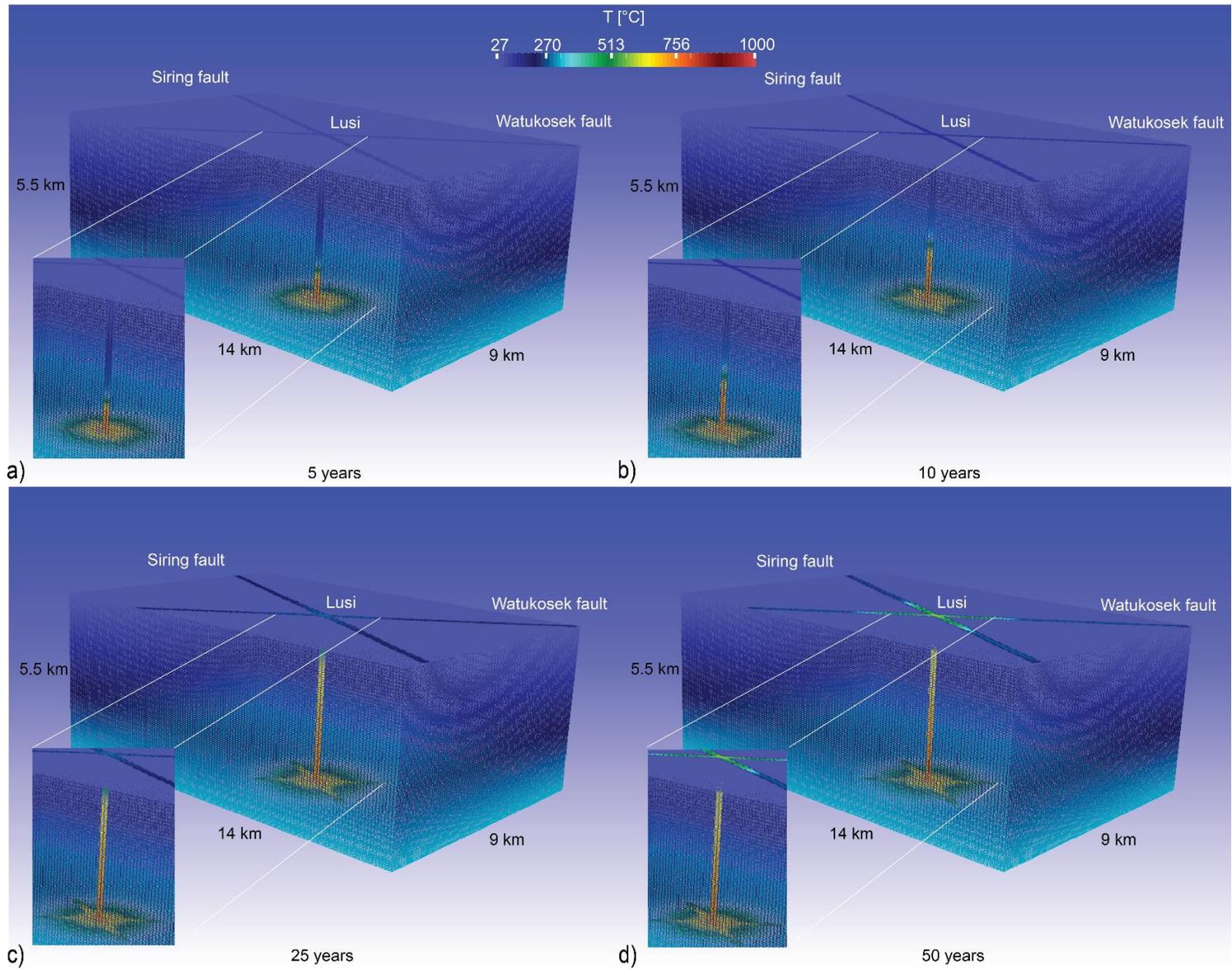
Figure 6

Figure 7

Figure 8

Figure 9

Figure 10

Figure 11